AIP | The Journal of Chemical Physics

Enhancement factor statistics of surface enhanced Raman scattering in multiscale heterostructures of nanoparticles

Gianluigi Zito, Giulia Rusciano, and Antonio Sasso

Citation: The Journal of Chemical Physics **145**, 054708 (2016); doi: 10.1063/1.4960179
View online: http://dx.doi.org/10.1063/1.4960179
View Table of Contents: http://scitation.aip.org/content/aip/journal/jcp/145/5?ver=pdfcov
Published by the AIP Publishing

Articles you may be interested in

Silicon nanowire arrays coated with electroless Ag for increased surface-enhanced Raman scattering
APL Mater. **3**, 056101 (2015); 10.1063/1.4921040

Dimensional scale effects on surface enhanced Raman scattering efficiency of self-assembled silver nanoparticle clusters
Appl. Phys. Lett. **105**, 073105 (2014); 10.1063/1.4893373

Surface enhanced fluorescence and Raman scattering by gold nanoparticle dimers and trimers
J. Appl. Phys. **113**, 033102 (2013); 10.1063/1.4776227

Multimodal plasmon coupling in low symmetry gold nanoparticle pairs detected in surface-enhanced Raman scattering
Appl. Phys. Lett. **98**, 183115 (2011); 10.1063/1.3555429

Plasmonic coupling of SiO 2 – Ag “post-cap” nanostructures and silver film for surface enhanced Raman scattering
Appl. Phys. Lett. **98**, 153103 (2011); 10.1063/1.3555342

Reuse of AIP Publishing content is subject to the terms: https://publishing.aip.org/authors/rights-and-permissions. Downloaded to IP: 91.252.167.84 On: Thu, 04 Aug 2016 20:13:45

Enhancement factor statistics of surface enhanced Raman scattering in multiscale heterostructures of nanoparticles

Gianluigi Zito,[a] Giulia Rusciano, and Antonio Sasso
Department of Physics Ettore Pancini, University of Naples Federico II, via Cintia, 80126-I Naples, Italy

(Received 26 April 2016; accepted 20 July 2016; published online 4 August 2016)

Suitable metal nanostructures may induce surface-enhanced Raman scattering (SERS) enhancement factors (EFs) large-enough to reach single-molecule sensitivity. However, the gap hot-spot EF probability density function (PDF) has the character of a long-tail distribution, which dramatically mines the reproducibility of SERS experiments. Herein, we carry out electrodynamic calculations based on a 3*D* finite element method of two plasmonic nanostructures, combined with Monte Carlo simulations of the EF statistics under different external conditions. We compare the PDF produced by a homodimer of nanoparticles with that provided by a self-similar trimer. We show that the PDF is sensitive to the spatial distribution of near-field enhancement specifically supported by the nanostructure geometry. Breaking the symmetry of the plasmonic system is responsible for inducing particular modulations of the PDF tail resembling a multiple Poisson distribution. We also study the influence that molecular diffusion towards the hottest hot-spot, or selective hot-spot targeting, might have on the EF PDF. Our results quantitatively assess the possibility of designing the response of a SERS substrate so as to contain the intrinsic EF PDF variance and significantly improving, in principle, the reproducibility of SERS experiments. *Published by AIP Publishing.* [http://dx.doi.org/10.1063/1.4960179]

The last decades have seen an exponential growth of attention and efforts regarding plasmonic nanostructures for their extraordinary capabilities of controlling sub-diffraction light and near-field amplification properties.[1] Surface-enhanced Raman scattering (SERS) spectroscopy represents one of the most important applications.[2] SERS, in fact, allows to resolve the chemical signature of molecules by means of localized surface plasmon-polariton resonances (LSPRs) which may enhance the near-field excitation and scattering from molecules of many orders of magnitude. This has prompted a plethora of SERS applications for molecular sensing in chemistry, biology, and medicine relying on the non-invasive and label-free nature of the approach.[3–8] Synergistically, advanced engineering of materials synthesis and lithographic nano-fabrication has allowed to develop and control the properties of LSPRs and their interaction in hybridized plasmonic structures,[9] Fano resonators, nanolenses, waveguides, nano-lasers, etc.[10]

Regarding molecular detection, an enormous boost to the research has followed the experimental evidence of single-molecule sensitivity achievable in SERS-active colloidal suspensions.[11,12] The most favorable enhancement sites, termed hot spots, are in the gaps between closely spaced nanoparticles (NPs) where the electromagnetic field is strongly localized. The electromagnetic contribution[13] to the SERS enhancement factor (EF) at a given position $\vec{r}$ is proportional, with good approximation, to the fourth power of the near-field gain $g(\vec{r}) = |(E_s(\vec{r}) + E_o(\vec{r}))/E_o(\vec{r})|$, where $E_s(\vec{r})$ and $E_o(\vec{r})$ are, respectively, the scattered and incident field amplitudes. Throughout the paper, we will assume $E_s(\vec{r}) \gg E_o(\vec{r})$. Therefore, the EF can be written as $G(\vec{r}) = g(\vec{r})^4 = |E_s(\vec{r})/E_o(\vec{r})|^4$. Typically $E_s(\vec{r})$ is a fast function of $\vec{r}$ close to the hottest spot where the maximum of the local field is achieved. Given the nanoscale geometry, the incident field can be approximated to a plane-wave illumination, hence $|E_o(\vec{r})| = E_o$. The maximum values of the SERS EF can reach $\sim 10^{12}$ to 10^{13} in favorable sites, occurring, e.g., in nanofocusing structures like self-similar chains of NPs (also termed nanolenses).[14] Such sites are thought to account for most of the experimental single-molecule detections achieved in random colloidal clusters.

The strong localization of the near-field is responsible for producing an extreme-value distribution of the SERS intensity when molecules randomly target a certain hot-spot. Le Ru *et al.* have shown that a Poisson distribution[11] is not a reliable SERS intensity distribution model in single molecule regime for several reasons.[15] A more realistic model relies on a long-tail distribution like a truncated Pareto distribution,[16] or a modified, phenomenological version with a further exponential factor to account for the averaging process over many hot-spots.[17,18] The phenomenological model explains the blurring of the cutoff of the EF distribution by assuming a collection of independent symmetric dimers with hot-spots of different strength. However, the behavior induced in asymmetric and multiscale plasmonic architectures of strongly coupled NPs, often met in experiments, has never been studied.

Herein, we show that while for a homodimer (HD) of NPs a truncated Pareto long-tail is a good model of EF statistics, plasmon coupling in adjacent concatenated nanoparticles of mismatched sizes produces a probability density function (PDF) of the EF with more complex properties. We also study

[a]E-mail: zito@fisica.unina.it. Tel.: (+39) 081 676273. Fax: (+39) 081676352.

Reuse of AIP Publishing content is subject to the terms: https://publishing.aip.org/authors/rights-and-permissions. Downloaded to IP: 91.252.167.84 On: Thu, 04 Aug 2016 20:13:45

the influence that molecular diffusion towards the hottest hot-spot, or selective hot-spot targeting, might have on the EF PDF.

We carried out electrodynamic calculations based on the 3D finite element method (FEM) of a self-similar trimer (SST) of NPs with the same geometric parameters as Ref. 14 in combination with Monte Carlo (MC) simulations of the random targeting of the nanostructure from analyte molecules. The SST was compared to a simple homodimer (HD) of NPs. While the HD has a single hot spot with a progressive (nonmonotonic) decay of the near-field far from the gap, the SST has a highly asymmetric spatial distribution of the near field with multiple hot-spots.

We considered spherical nanoparticles of silver with the dielectric function from Johnson and Christy.[19] The radii of the NPs of the trimer were $R^{(t)}_{\{1,2,3\}} = \{30, 10, 3.3\}$ nm for $NP_{1,2,3}$ in this order, with gaps measured between the closest points of NP_1 and NP_2, and NP_2 and NP_3, respectively, given by $d_{\{12,23\}} = \{6, 2\}$ nm. For the HD, we set the radii $R^{(d)}_{\{1,2\}} = 30$ nm and the gap to $d = 2$ nm. Both systems were embedded into a medium with refractive index $n = 1.41$ (like a polymer with Raman analytes dispersed in it). We considered a plane wave illumination with polarization parallel to the systems axis. The overall spherical domain of simulation had a radius of 400 nm with perfectly matched layer (PML) and scattering boundary conditions.[20] The spatial distribution of EF was calculated according to the fourth-power model considering the norm of the total scattered field, as such we intend $E_s(\vec{r}) = \|\vec{E}_s(\vec{r})\|$. An auxiliary surface enclosing radiating NPs was used to calculate the scattering cross section (SCS) spectra, while the absorption cross section (ACS) was calculated considering the resistive loss integrated over the NPs volume.[20,21] An extra-fine FEM-based mesh was used with minimum element size of 0.07 nm. Calculation was carried out in the frequency domain, with wavelength sweep step of 2.5 nm (0.2 nm for finer inspections). The spatial distribution of the electromagnetic field was verified to be stable with respect to the mesh density. The spherical PML shell was chosen thick-enough to ensure no backreflection of the incident field, with attenuation of about a factor 10^5. Further details of calculation can be found in Refs. 5 and 22.

In Figure 1(a), we show the total SCS and ACS produced by the SST. In particular, we focused our attention on two plasmon modes of the system, the subradiant mode (yellow arrow) and the superradiant mode (blue arrow). In Figures 1(b) and 1(c), the midplane EF distributions (white-to-red colormap), indicated as *G*-maps, are plotted for the subradiant and superradiant mode, respectively. In the same figures, also the NP surface charge density Σ eigenmodes supported by the SST at these two wavelengths are depicted (blue-to-red colormap). In the case of the localized surface plasmon (LSP) at 455 nm (Figure 1(c)), the associated dipole moments on all nanoparticles are aligned and in phase, so that the LSP mode couples well to the external field and forms a superradiant or bright mode. The LSP in Figure 1(b) is instead characterized by antiparallel dipole moments between NP_1 and the subsystem consisting of NP_2 and NP_3, which corresponds to a subradiant, weakly dark mode, associated with the dip at 420 nm in the SCS spectrum (Figure 1(a)). To

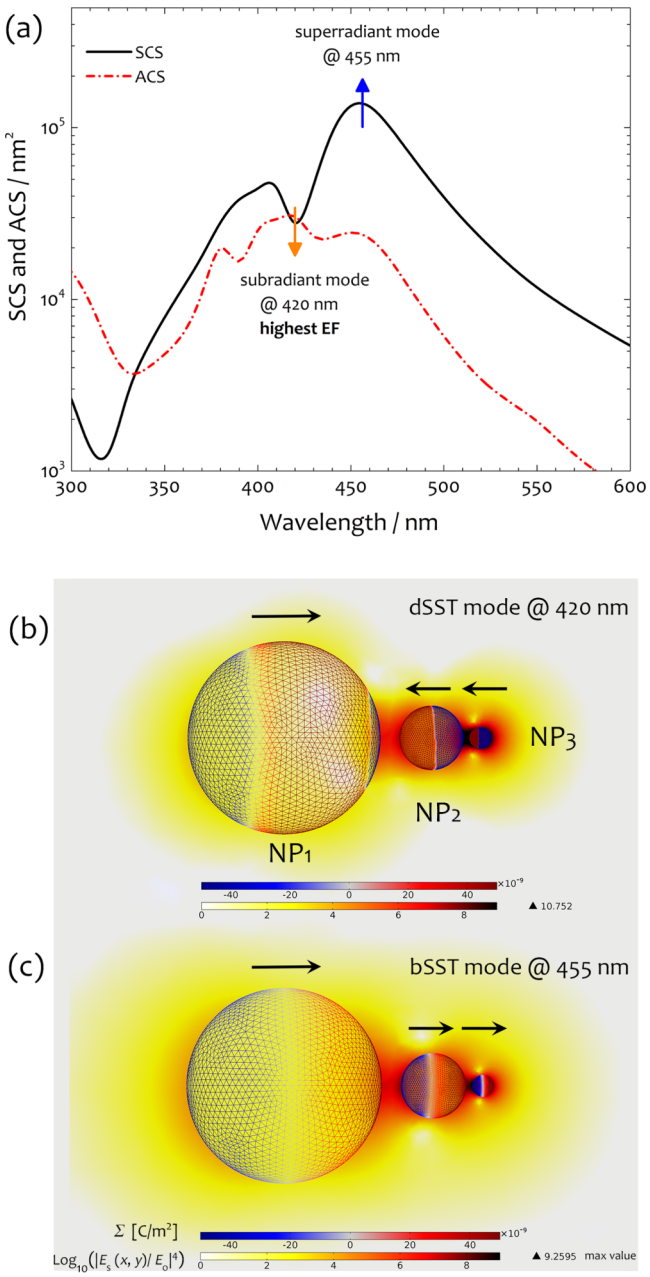

FIG. 1. (a) Total SCS and ACS for the self-similar trimer. (b) *G*-map in the midplane of the SST (white to red) and surface-charge density distribution Σ wireframed over the NP surfaces (blue to red) at the subradiant mode at 420 nm (indicated as dSST). (c) Same as in (b) at the superradiant mode at 455 nm (bSST). The arrows indicate NP dipole moment orientation.

distinguish these specific modes of the self-similar trimer, we will indicate them, respectively, as bSST (bright) and dSST (dark).

As visible from the *G*-maps, the near-field spatial distributions are modulated by the specific Σ eigenmodes. In Figure 2, the EF distribution of the SST at these wavelengths is further emphasized over the NP surfaces with a different color scale for dSST (Figure 2(a)) and bSST (Figure 2(b)) and compared to the homodimer's (Figure 2(c)). For the latter, we plot the *G*-map showing the maximum EF, i.e., at the spectral position corresponding to the dipole (bright) resonance in the HD scattering spectrum, which occurs at 580 nm (data not shown). For the HD, the symmetric simple structure gives

Reuse of AIP Publishing content is subject to the terms: https://publishing.aip.org/authors/rights-and-permissions. Downloaded to IP: 91.252.167.84 On: Thu, 04 Aug 2016 20:13:45

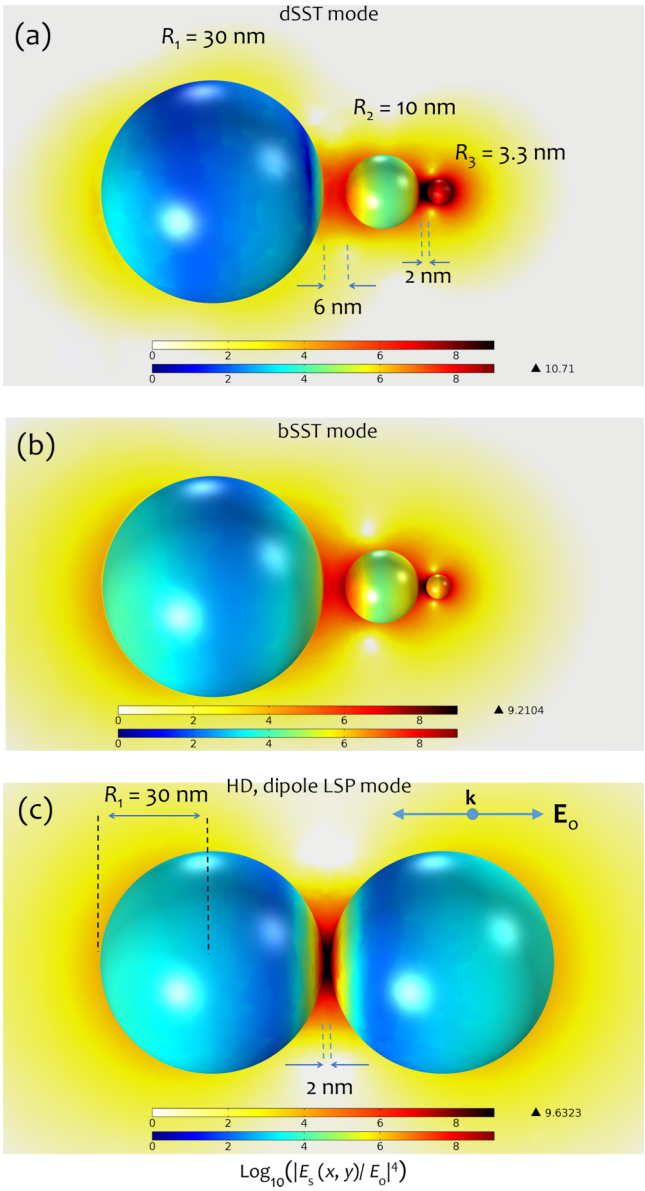

FIG. 2. (a) G-map in the midplane (thermal colormap, white to red) of the SST at subradiant mode (420 nm) and over the NP surfaces (rainbow colormap, blue to red); the different scales emphasize field variations. (b) Same as in (a), but at the superradiant mode (455 nm). Same as in (a), for the HD at the dipole LSP occurring at 580 nm (i.e., the mode showing the maximum EF).

rise to a well defined gap hot-spot rapidly fading over the NP surfaces and surrounding space moving far from the gap-center (Figure 2(c)).

In the case of the SST, as well-known, the nanofocusing effect gives rise to a large field enhancement with multiscale variation (Figures 2(a) and 2(b)). As a result of the hybridized LSP response of the three NPs, the EF is actually leveled on three different scales: 10^2–10^4 (NP_1, mainly blue), 10^4–10^8 (NP_2, mainly green), and $>10^8$ (NP_3, mainly red) (Figure 2(a)). The cascade progression is unilateral and proceeds always from the biggest NP toward the smallest one, regardless of the excitation wavelength, so that the maximum local field is in the smallest gap d_{23} (Figures 2(a) and 2(b)). However, specific eigenmodes also determine specific EF distribution over the NP surfaces. For example, we can see how the EF distributions on NP_1 and NP_3 change from Figure 2(a) to Figure 2(b). The spectral position that shows the maximum amplification is not the bright resonance bSST at 455 nm but the weakly dark mode bSST at 420 nm, which has $G_{max} = g^4_{max} = 475^4 \simeq 5.1 \times 10^{10}$ (Figure 2(a)) against $G_{max} = 200^4 \simeq 1.6 \times 10^9$ of the former (Figure 2(b)). It is also worth mentioning that the extreme local field enhancement for the dSST is inferior to what predicted in Ref. 14 probably because of retardation effects included in our electrodynamic computation. In fact, just reducing the overall scale of the trimer of 20% gives an improved $G_{max} \simeq 3.5 \times 10^{11}$ at the subradiant mode (data not shown here).

The particular near-field response of the SST reflects a general behavior associated to the symmetry breaking of the geometry. In fact, the near field distribution that arises in coupled NPs may be strongly affected by the system symmetry and the hybridization of the plasmonic response.[22–24] In addition, in any realistic structure the symmetry is usually broken, especially when considering more than two NPs as in the common case of SERS-active colloidal aggregates. Therefore, in a complex metal nanostructure, multiscale regions of EF or multiple hot-spots, with close or well-separated amplifications, can be found and tangled in unconventional ways as a result of the strong coupling and specific geometry.

In the following, we will focus our MC simulations considering the spatial distribution of the enhancement factor shown in Figures 2(a)-2(c) by simulating the random adsorption of analyte molecules targeting the proximity regions to the metal nanosurfaces. MC simulations were carried out following the same basic idea proposed by Le Ru *et al.*[16] However, we virtually probed the EF distribution by extracting random discrete positions $\vec{r}_i$ (with index i defined below) from the $3D$ domain of simulation with no approximations on the EF spatial dependence. To this end, we followed two strategies: in the first, the molecules were distributed over the NP surfaces, i.e., the positions $\vec{r}_i$ were extracted from the surfaces enclosing the NPs having radii $R^{(d,t)} + 0.5$ nm; whereas, in the second, the positions $\vec{r}_i$ were extracted from all the volume around the NPs. In more detail, we discretized homogeneously the space in voxels as large as a typical molecular volume $V_{probe} = 0.6$ nm^3 (approximating the Raman-resonant crystal violet volume) and surface pixels of area $A_{probe} = 0.85$ nm^2. Herein, we will discuss mainly the case of molecules adsorbed only to the NP surfaces, however both cases were simulated and compared. We first consider the case of molecules uniformly targeting the surfaces of the NPs, which have, in other words, the same *a priori* probability of being covered by a molecular probe. Therefore, this probability is affected only by the extension of the surface of each NP. The EF statistics was built by extracting N_m random positions from the EF spatial distribution grid. This last was obtained by interpolating the electromagnetic field values of the simulation mesh to achieve a uniform grid density.

A variable number N_m of molecules, i.e., spatial coordinates $\vec{r}_i$, was simulated from $N_m = 1$ up to a maximum value given by the pack density limit of 0.625 V_u/V_{probe}, where V_u is the volume of the region surrounding the

Reuse of AIP Publishing content is subject to the terms: https://publishing.aip.org/authors/rights-and-permissions. Downloaded to IP: 91.252.167.84 On: Thu, 04 Aug 2016 20:13:45

NPs (for surface targeting the maximum N_m was of the order of 10^4). In order to build the statistics of the EF, we generated a number $N = 10^5$ of events, each of which consisting of a random set $\{\vec{r}_1, \vec{r}_2, \ldots, \vec{r}_i, \vec{r}_{i+1}, \ldots, \vec{r}_{N_m}\}$. The detectable SERS intensity $I_{S,j}$ of the jth event of a collection of N events is proportional to the enhancement factor according to the 4-th power approximation. First, we will consider the case $G(\vec{r}) = g(\vec{r})^4 = |E_s(\vec{r})/E_o(\vec{r})|^4$, which implies that the Raman frequency ω_R is close-enough to the laser frequency ω_L so that $E_s(\omega_R) \simeq E_s(\omega_L)$, then we will release this hypothesis and make use of the more general relation $G(\vec{r}) = g(\vec{r};\omega_L)^2 g(\vec{r};\omega_R)^2$. Therefore, for each event of the MC simulation, we can write

$$G_j = \frac{1}{N_m} \sum_{i=1}^{N_m} g(\vec{r}_i)^4 \quad \text{for} \quad j = 1, \ldots, N \tag{1}$$

where $g(\vec{r}_i)$ represents the field gain at the position $\vec{r}_i$ randomly probed by the ith molecule. Therefore, G_j is, accordingly, the enhancement detected at the jth event and given by the superposition of the random set of positions covered by N_m molecules. Also for the MC simulations, the enhancement factor G was calculated considering the norm of the total scattered field (unpolarized detection).

Once N values of G_j are acquired, the probability density function of the enhancement factor can be built as the histogram of G_j. Such a histogram can be seen as a function of N_m. We considered a number of events $N = 10^5$ and built the statistics of the EF for increasing values of N_m, in accord with Ref. 16. In Figures 3(a) and 3(b), we plot, respectively, the PDFs determined for the homodimer at its dipole resonance at 580 nm, and for the self-similar trimer at 420 nm (dSST mode). The corresponding G-maps are shown, respectively, in Figures 2(c) and 2(a). We considered molecules adsorbed only to the NP surfaces. The histogram bin spacing was logarithmic with a number of bins equal to $\sqrt{N}$ for all PDFs. The conclusions inferred hold also in the case of linear binning, however the logarithmic one is more effective.

The dimer shows the typical long tail statistics of a gap hot-spot that can be truncated, for large enough values of G, to a Pareto power law with good approximation.[16] In particular, in Figure 4(a) we show the fit of the long tail for $N_m = 1$. The value of the coefficient k obtained from the fit, $k = 0.15 \pm 0.02$, is in good agreement with what reported in Ref. 16. Inspecting Figure 3(a), we can also see that the PDF of the homodimer reaches a nearly symmetric Gaussian distribution for $N_m = 2 \times 10^3$, i.e., for a surface coverage $f \simeq 7.5\%$. The corresponding average is $\langle G \rangle = 7.0 \times 10^6$ and, of course, coincides with the spatial average EF calculated from the near-field solution. The relative standard deviation $\sigma_r = \Delta G/\langle G \rangle$ becomes $\simeq 15.6\%$ for a larger surface fraction coverage with $N_m = 10^4$ ($f \simeq 38\%$).

The self-similar trimer shows quite a different behavior. Clearly, disconnected regions emerge in the PDF and the overall PDF has a larger slope with respect to the dimer's. The zones in the PDF can be associated to the peculiar spatial distribution of the EF over the NP surfaces characterized by a well-defined multiscale variation of field gain prompted by the SST geometry (Figure 2(a)). We ascertained this by simulating also the PDF taking the NPs one by one but with G-maps resulting from the whole coupled trimer. This allowed us to identify specific ranges of EF as associated to the G-values present on NP_1, NP_2, and NP_3 (Figure 3(b), $N_m = 1$). In addition, given the multiparticle coupling of the trimer, there are areas of the surfaces of NP_2 and NP_3 that show a comparable level of EF, which in turn produces a sort of peaks in the pattern of the PDF. In addition, in Figure 4(b), we show the fit of the approximated (and smoothed) long-tail statistics obtained for the trimer, for $N_m = 1$ (same as Figure 3(b)). Although not properly a single long-tail statistics, we still can obtain the coefficient k from the fit, which is in this case largely affected by the different scaling of the electromagnetic field and gives a value $k = 0.30 \pm 0.02$, i.e., doubled with respect to the HD case reported in Figure 4(a). Returning to Figure 3(b), we can see that the PDF of the SST converges to a nearly symmetric distribution for $N_m = 2 \times 10^3$ and then reaches a narrower symmetric Gaussian distribution with $\sigma_r \simeq 23\%$ for $f = 65\%$. In this case, $\langle G \rangle = 2.3 \times 10^7$, i.e., only a factor ~3 larger than the average EF of the dimer, but with maximum EF nearly one order of magnitude larger, and mainly concentrated around the smallest NP_3.

Given the different geometries of HD and SST, instead of comparing $\langle G \rangle$, it is useful to introduce the figure of merit $\eta = \langle G \rangle/(f\sigma_r)$, which accounts for the different surface coverage and strength of the hot-spot implicit in f and $\langle G \rangle$, respectively. The product $\langle G \rangle(1/\sigma_r)$ combines metrics for good enhancement and good reproducibility. However, the reproducibility measured by $1/\sigma_r$ is a monotonically increasing function of f. Therefore, the comparison of $\langle G \rangle(1/\sigma_r)$ between different substrates must be done at the same level of f. In addition, if two substrates give the same ratio $\langle G \rangle/\sigma_r$, both with comparable and low σ_r (indication of a reliable sensing), the SERS substrate reaching that ratio with the smallest f should be preferred because that substrate allows good sensing for lower molecular density, which can be useful for trace detection. Furthermore, the normalization with respect to f might be useful, practically, because the molecular surface coverage achieved in two experiments may be different. Therefore, we considered η as a reasonable choice for comparing the properties of different SERS substrates. In Table I, we report some relevant parameters of the EF distribution for the cases of the HD, dSST and bSST modes under the assumption of uniform molecular targeting previously mentioned.

In Figures 5(a) and 5(b), we compare the EF PDFs, respectively, obtained in the case of the subradiant mode with that produced by the superradiant mode of the self-similar trimer. In addition, these time data are reported in linear scale (with logarithmic binning) to emphasize how structured patterns arising in the PDF may resemble a Poisson distribution. Figure 5(a) reports the same data as Figure 3(b). If we consider, e.g., Figure 5(a), case $N_m = 500$, a pattern of peaks is clearly visible in the PDF. However, this is not associated to molecular counting[11] but only to the structured distribution of the EF produced by the specific near-field response provided by the trimer at 420 nm.

Reuse of AIP Publishing content is subject to the terms: https://publishing.aip.org/authors/rights-and-permissions. Downloaded to IP: 91.252.167.84 On: Thu, 04 Aug 2016 20:13:45

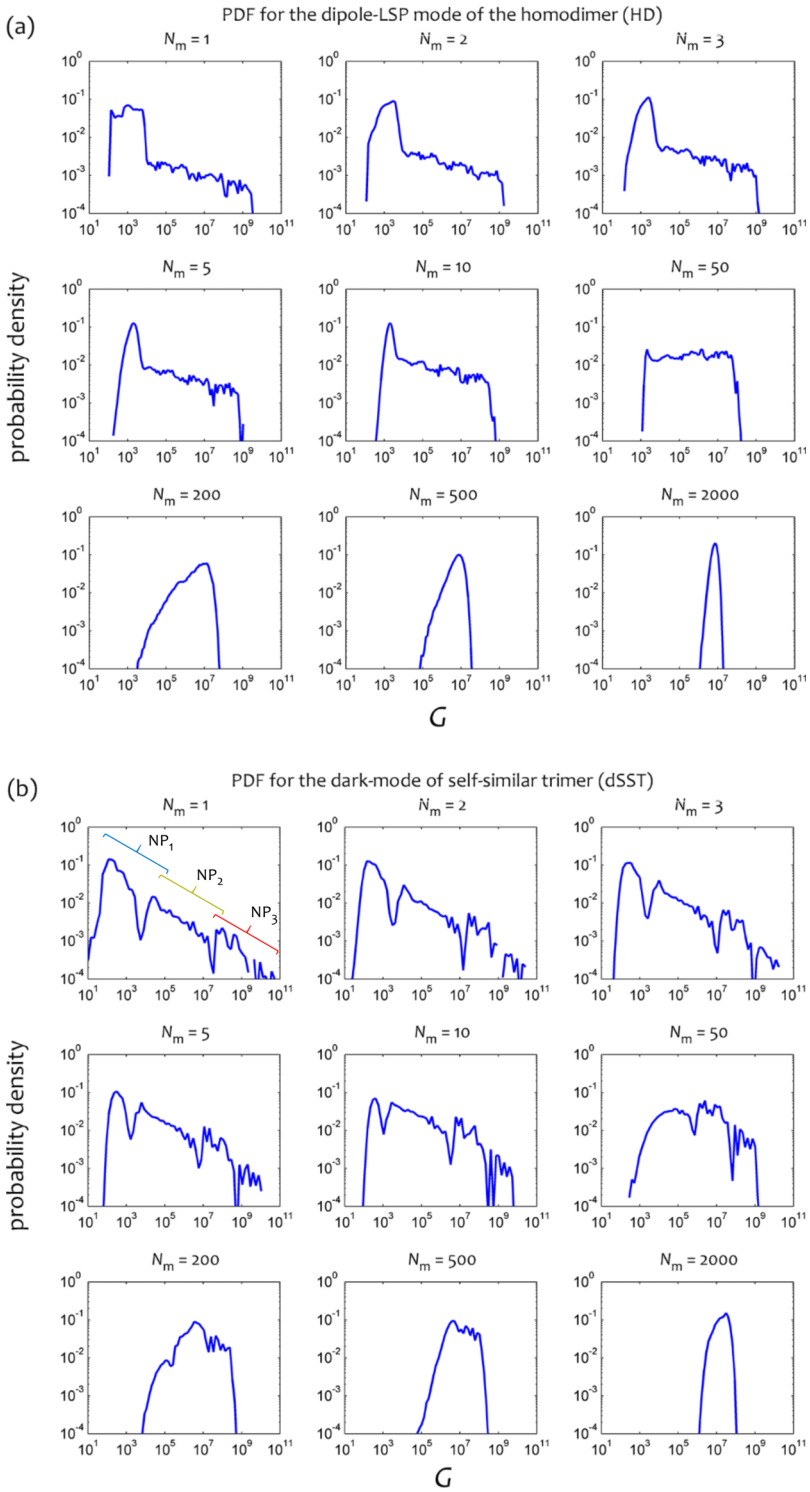

FIG. 3. (a) PDFs obtained as a function of N_m at the HD's dipole mode; and (b) for the self-similar trimer at its subradiant mode (dSST).

The PDF changes when considering the second LSP mode (bSST, Figure 5(b)). Not only is the slope of the asymmetric PDF modified by the different strength of the hot-spot of this mode (please note the different range of G in Figure 5(b)), but the pattern emerging in the PDF also changes in correspondence to the variations in the G-map over the NP surfaces. The parameters associated with the PDF are summarized in Table I (bSST uniform targeting). The overall efficiency measured by η is much less than both SST dark mode's (dSST uniform targeting) and homodimer's (HD uniform targeting). It is interesting to notice that the EF distribution parameters eventually indicate the simple HD structure to be much more performant than the complex SST when both are taken at their respective maxima of the scattering spectrum (lower energy dipole plasmon resonance). This suggests that a rational design of the SERS substrate structure and its near-field spectral response, also in terms of intrinsic reproducibility (σ_r) and overall efficiency (η), instead of maximum EF achievable, could be experimentally more useful.

Finally, it is worth mentioning that the patterns in the PDFs were still present, although with minor contrast, also in

Reuse of AIP Publishing content is subject to the terms: https://publishing.aip.org/authors/rights-and-permissions. Downloaded to IP: 91.252.167.84 On: Thu, 04 Aug 2016 20:13:45

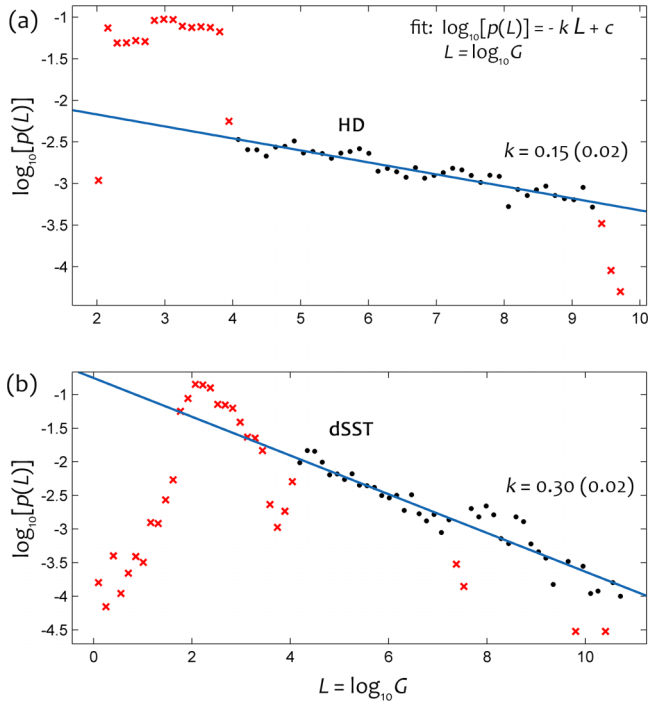

FIG. 4. Fit of the long tail pdf for $N_m = 1$ for the HD (a) and dSST mode (b). Red points were ignored for the fit. The coefficient k is consistent with the definition of Ref. 16 and in good agreement with that expected for a truncated Pareto power-law for the case reported in (a).

the case of molecules randomly targeting the whole accessible volume surrounding the NPs (the volume included all the space with SERS amplification in the range $[1, G_{max}]$).

Since different modes (dSST and bSST) give rise to different PDFs, if we consider an excitation wavelength at 420 nm (dSST) and a Raman frequency shift of 1832 cm^{-1}, i.e., at 455 nm (bSST), a more appropriate approach for calculating the EF statistics is using the relation $G(\vec{r}) = g(\vec{r};\omega_L)^2 g(\vec{r};\omega_R)^2$. This is done in Figure 6, where the resulting PDFs still show a structure of peaks (see, e.g., $N_m = 50$ and 200) that results from the combination of the two statistics of the dSST and bSST modes. Combining the two different modes (excitation and Raman frequencies) does not smooth the structured tail mainly because the near-field produced by the SST at different wavelengths has always the same asymmetric character (see Figures 2(a) and 2(b)). The average enhancement factor reaches a compromise between the two modes and is equal to $\langle G \rangle = 1.4 \times 10^6$. Reproducibility, instead, appears even worse ($\sigma_r = 27\%$) (Table I). Also in this case, the coefficient k ($N_m = 1$) obtained from a fit of the smoothed long tail for $G > 10^4$ (as reported in Figure 4) gave a value not comparable with the HD's, being $k = 0.35 \pm 0.04$. This, in fact, was mainly influenced by the PDF of the bSST, for which we found $k = 0.36 \pm 0.03$ (calculation carried using the approximation $\omega_L \simeq \omega_R$ in analogy to the case dSST shown in Figure 4(b)).

TABLE I. Characteristic parameters of the EF derived for the homodimer (HD) and the self-similar trimer at the subradiant, dark mode (dSST), and bright mode (bSST) for different molecular targeting condition: uniform targeting, diffusion towards hot-spots, and selective targeting. For all $\omega_L \simeq \omega_R$, except for row 4, where ($\omega_L \neq \omega_R$).

	$\langle G \rangle$	N_m	f (%)	σ_r (%)	η
HD uniform targeting	7.0×10^6	10^4	38	15.6	1.2×10^8
bSST uniform targeting	3.9×10^5	10^4	65	9.6	6.4×10^6
dSST uniform targeting	2.3×10^7	10^4	65	23.0	1.5×10^8
dSST (ω_L) and bSST (ω_R) unif. target.	1.4×10^6	10^4	65	27.0	8.0×10^6
dSST diffusion toward hot-spots	5.1×10^8	10^4	65	8.4	9.3×10^9
dSST selective targeting	1.5×10^9	20	14	12.0	8.9×10^{10}

Thus far, we have considered the case of molecules uniformly targeting the surfaces of the NPs. In other words, we have conjectured that each point of the substrate surface has the same *a priori* probability of being covered by a molecular probe. In the following, we release this hypothesis and discuss two examples of nonuniform molecular targeting.

(i) For SERS-substrates in liquid, it is not unlikely that molecules may diffuse towards specific sites of the nanostructures. In several cases, it has been argued that molecules may actually diffuse towards the hottest hot-spot.[12] Therefore, we introduced a weight-function to balance the mismatching of NP areas in the self-similar scaling to simulate a molecular diffusion towards the hottest hot-spot. To do so, we simply favored the targeting of the hotter regions by virtually increasing the probability of adsorption on NP_2 and NP_3 of a factor 9 and 81, respectively, with respect to NP_1 (unchanged). This scaling was artificial and not supported by a particular diffusion model. The factors 9 and 81 were only intended to balance the different surface area between the three NPs (whose radii scale by a factor 3), so that each NP, regardless of its actual surface, collected the same number of molecules.

(ii) The second nonuniform targeting considered is the following. As demonstrated by Le Ru *et al.*,[25] guiding the molecules to probe only the regions of the NPs where the maximum EF is achieved, by virtue of a proper functionalization, might improve the detection efficiency of single-molecule events. From a quantitative standpoint, how much can SERS reproducibility improve by a SERS substrate synergistically engineered to limit the PDF variance? To answer this question for the case of the SST here discussed, we imagined a selective adsorption of molecules only toward the NP_3, having in mind the idea of a specific chemical functionalization capable of attracting and capturing molecules on it as in the case of immunotargeted NPs.

The results of these two MC simulations are reported in Figure 7 for the most significant case of the dSST mode showing the largest EF. The corresponding parameters of the EF statistical distribution are reported in the last two rows of Table I.

(i) Comparing Figure 7(a) with the former case of uniform molecular targeting reported in Figure 5(a) (same EF spatial distribution, dSST), it is clear that the hypothesis of diffusion towards the regions of larger EF on NP_2 and NP_3 alters dramatically all parameters of the EF statistics: the distribution becomes symmetric for a lower number of

Reuse of AIP Publishing content is subject to the terms: https://publishing.aip.org/authors/rights-and-permissions. Downloaded to IP: 91.252.167.84 On: Thu, 04 Aug 2016 20:13:45

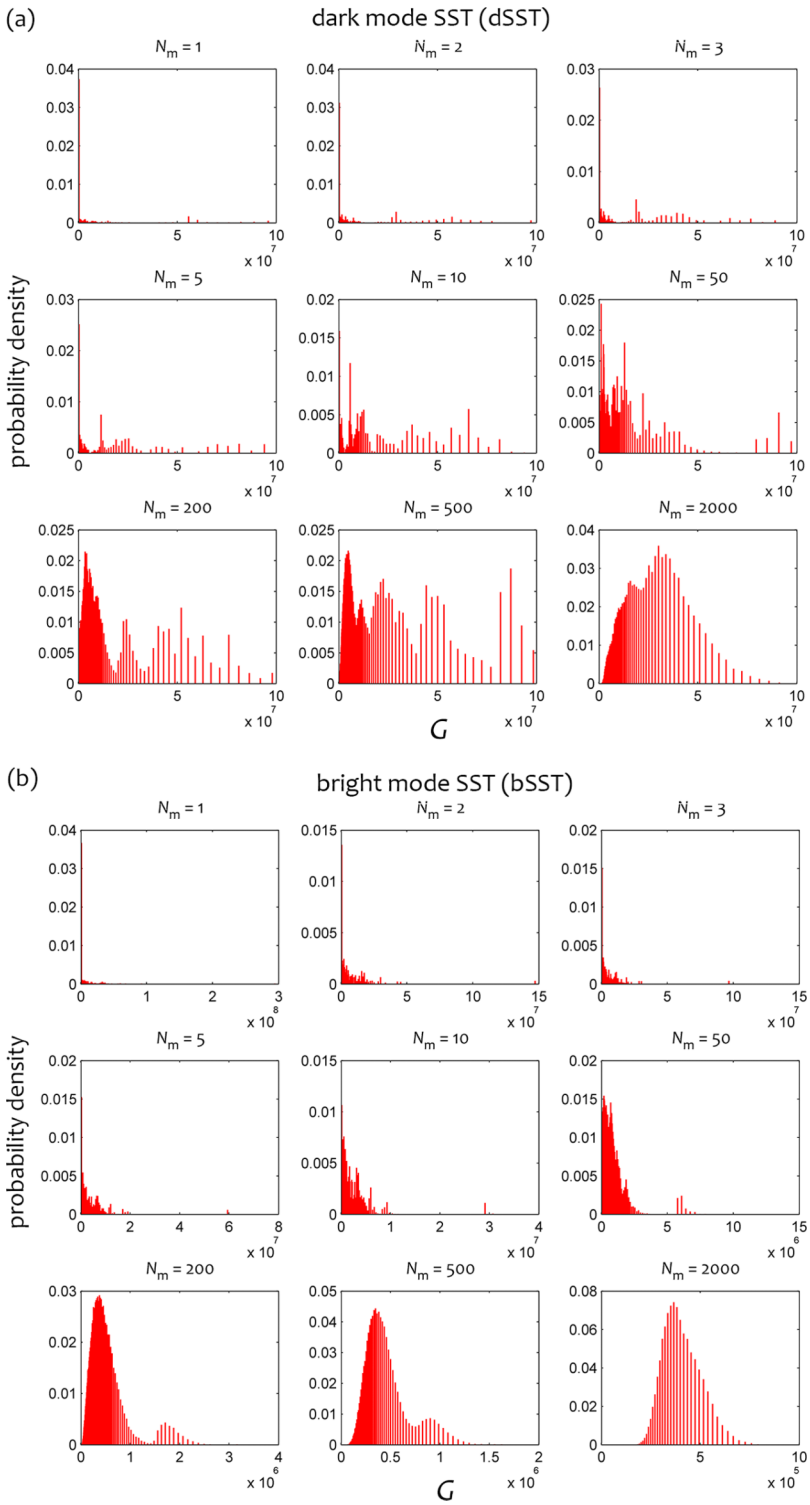

FIG. 5. (a) PDFs obtained as a function of N_m for the SST at the subradiant mode (420 nm); and (b) at the superradiant mode (455 nm). Please note that here we use linear scales on the axes but again a logarithmic bin spacing for the histograms. For low N_m, most of data events are hidden by x and y axes.

molecules; the mean value of EF is larger of one order of magnitude (Table I); the reproducibility (σ_r) improves, and the overall efficiency η increases of a factor 62.

(ii) Even more dramatic is the apparent behavior of the SERS EF of the SST when molecules selectively adsorb only to the region of largest EF, i.e., NP_3 (Figure 7(b)). It is remarkable that with only 20 molecules, corresponding to a relative low surface fraction coverage $f = 14\%$, not only the average EF is extremely large, $\langle G \rangle = 1.5 \times 10^9$, but also the symmetric Gaussian distribution is very narrow, being $\sigma_r = 12\%$. In this case, the overall efficiency η of the SERS substrate improves by a factor 593 with respect to the case of uniform targeting of the SERS substrate. This result points out the possibility of improving the intrinsic reproducibility and efficiency of SERS experiments of even three orders of magnitude by virtue of a suitable design of the specific response of the SERS substrate, which would be desirable for most analytic applications that make use of surface-enhanced Raman scattering sensing.

Reuse of AIP Publishing content is subject to the terms: https://publishing.aip.org/authors/rights-and-permissions. Downloaded to IP: 91.252.167.84 On: Thu, 04 Aug 2016 20:13:45

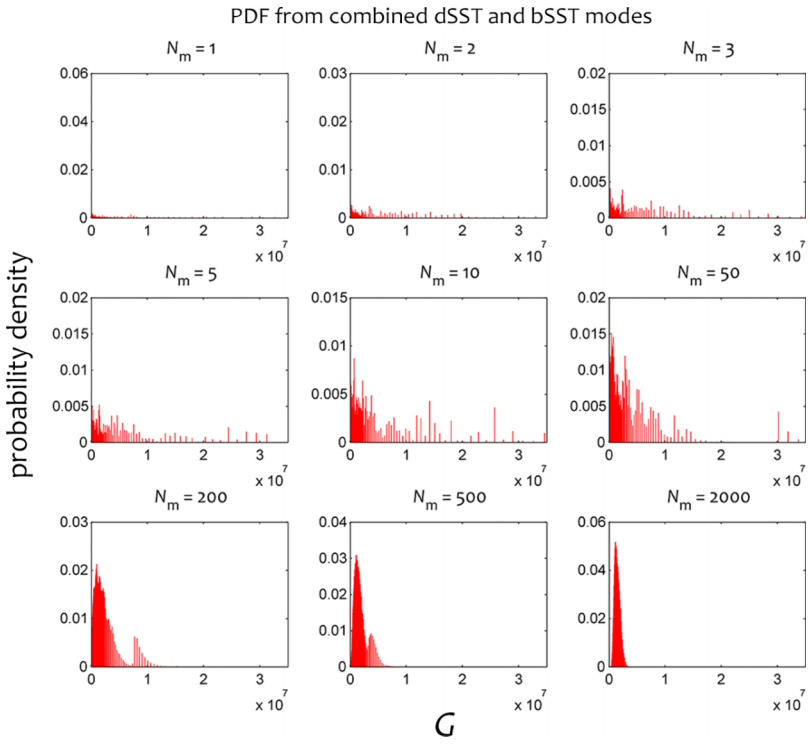

FIG. 6. PDFs obtained as a function of N_m for combined dSST and bSST modes.

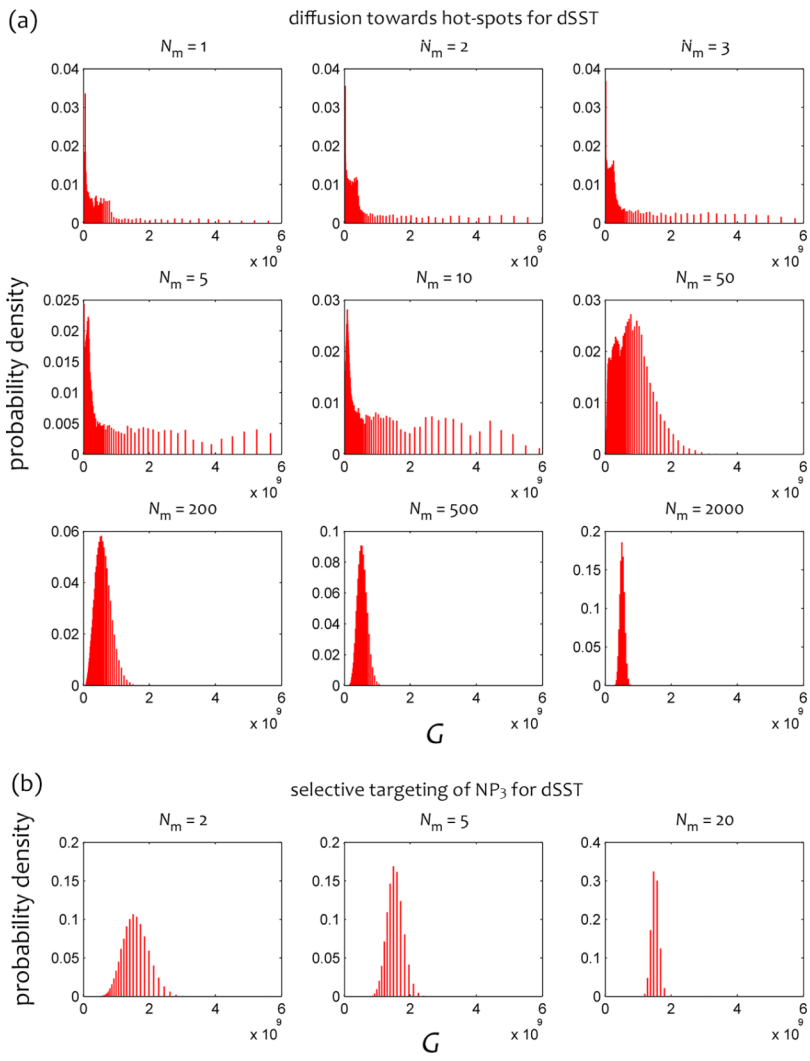

FIG. 7. (a) PDFs obtained as a function of N_m for the SST at the subradiant mode (420 nm) under the assumption of a characteristic molecular diffusion towards the hot-spots; and (b) selective targeting of NP_3 (surface of largest EF).

Reuse of AIP Publishing content is subject to the terms: https://publishing.aip.org/authors/rights-and-permissions. Downloaded to IP: 91.252.167.84 On: Thu, 04 Aug 2016 20:13:45

In summary, we have investigated the near-field response and SERS EF statistics of two plasmonic systems, a homodimer of NPs and a self-similar chain of three NPs. We have demonstrated that the broken symmetry of the plasmonic trimer induces particular modulations of the probability density function of the enhancement factor that resemble a multiple Poisson distribution. However, the structured patterns emerging in the PDF are not related to molecular counting but to the highly structured spatial distribution of the electromagnetic field on the NP surfaces and surrounding volume. The bottom line is that the statistics of the EF cannot be uniquely identified with the gap hot-spot statistics of a simple dimer. A phenomenological model[17,18] based on independent dimers, in general, does not take into account that the coupling between polydispersed NPs may give rise to behaviors much different from the simple case of homodimer of NPs. In addition, the particular PDF depends on the LSP resonance because the surface-charge density mode supported by the system at a particular excitation wavelength determines the spatial distribution of the local electromagnetic field and this in turn is reflected in the PDF.

Furthermore, our study points out that a suitable design of the SERS EF response may limit the intrinsic PDF variance so as to achieve a very reproducible SERS signal even in few-molecules regime (Figure 7(b)). With regard to the self-similar trimer here discussed, an array of chemically functionalized elements, e.g., fabricated with the approach proposed in Ref. 26, could produce, in principle, a quantitative, intrinsically reproducible SERS response also in single-molecule regime, provided that the molecules are conveyed to the hottest hot-spot.

G.Z. and G.R. acknowledge financial support from Italian Ministry of Education, University and Research (MIUR), Grant No. FIRB 2012-RBFR12WAPY; and in part from University of Naples Federico II, Compagnia di San Paolo e Istituto Banco di Napoli - Fondazione, STAR Project: LARA; A.S. acknowledges financial support from MIUR, Project No. MONICA PON01 0152.

[1]S. A. Maier, *Plasmonics: Fundamentals and Applications* (Springer Science & Business Media, 2007).
[2]E. Le Ru and P. Etchegoin, *Principles of Surface-Enhanced Raman Spectroscopy: And Related Plasmonic Effects* (Elsevier, 2008).
[3]J. Ando, T.-a. Yano, K. Fujita, and S. Kawata, Phys. Chem. Chem. Phys. **15**, 13713 (2013).
[4]L. Rodríguez-Lorenzo, R. de La Rica, R. A. Álvarez-Puebla, L. M. Liz-Marzán, and M. M. Stevens, Nat. Mater. **11**, 604–607 (2012).
[5]G. Zito, G. Rusciano, G. Pesce, A. Dochshanov, and A. Sasso, Nanoscale **7**, 8593–8606 (2015).
[6]C. De Rosa, F. Auriemma, C. Diletto, R. Di Girolamo, A. Malafronte, P. Morvillo, G. Zito, G. Rusciano, G. Pesce, and A. Sasso, Phys. Chem. Chem. Phys. **17**, 8061–8069 (2015).
[7]G. Rusciano, G. Zito, R. Isticato, T. Sirec, E. Ricca, E. Bailo, and A. Sasso, ACS Nano, **8**, 12300–12309 (2014).
[8]M. P. Cecchini, V. A. Turek, J. Paget, A. A. Kornyshev, and J. B. Edel, Nat. Mater. **12**, 165–171 (2012).
[9]N. J. Halas, S. Lal, W.-S. Chang, S. Link, and P. Nordlander, Chem. Rev. **111**, 3913–3961 (2011).
[10]J. A. Schuller, E. S. Barnard, W. Cai, Y. C. Jun, J. S. White, and M. L. Brongersma, Nat. Mater. **9**, 193–204 (2010).
[11]K. Kneipp, Y. Wang, H. Kneipp, L. T. Perelman, I. Itzkan, R. R. Dasari, and M. S. Feld, Phys. Rev. Lett. **78**, 1667 (1997).
[12]J. Kneipp, H. Kneipp, and K. Kneipp, Chem. Soc. Rev. **37**, 1052–1060 (2008).
[13]H. Xu, J. Aizpurua, M. Käll, and P. Apell, Phys. Rev. E **62**, 4318 (2000).
[14]K. Li, M. I. Stockman, and D. J. Bergman, Phys. Rev. Lett. **91**, 227402 (2003).
[15]P. G. Etchegoin, M. Meyer, and E. Le Ru, Phys. Chem. Chem. Phys. **9**, 3006–3010 (2007).
[16]E. Le Ru, P. Etchegoin, and M. Meyer, J. Chem. Phys. **125**, 204701 (2006).
[17]E. Le Ru and P. Etchegoin, J. Chem. Phys. **130**, 181101 (2009).
[18]Y. Fang, N.-H. Seong, and D. D. Dlott, Science **321**, 388–392 (2008).
[19]P. B. Johnson and R.-W. Christy, Phys. Rev. B **6**, 4370 (1972).
[20]V. Giannini, A. I. Fernández-Domínguez, S. C. Heck, and S. A. Maier, Chem. Rev. **111**, 3888–3912 (2011).
[21]C. F. Bohren and D. R. Huffman, *Absorption and Scattering of Light by Small Particles* (John Wiley & Sons, 2008).
[22]G. Zito, G. Rusciano, and A. Sasso, Opt. Express **24**, 13584–13589 (2016).
[23]A. Lovera, B. Gallinet, P. Nordlander, and O. J. Martin, ACS Nano **7**, 4527–4536 (2013).
[24]S. Chen, L.-Y. Meng, H.-Y. Shan, J.-F. Li, L. Qian, C. T. Williams, Z.-L. Yang, and Z.-Q. Tian, ACS Nano **10**, 581–587 (2016).
[25]E. C. Le Ru, J. Grand, I. Sow, W. R. Somerville, P. G. Etchegoin, M. Treguer-Delapierre, G. Charron, N. Félidj, G. Lévi, and J. Aubard, Nano Lett. **11**, 5013–5019 (2011).
[26]X. Liu, S. Biswas, J. W. Jarrett, E. Poutrina, A. Urbas, K. L. Knappenberger, R. A. Vaia, and P. F. Nealey, Adv. Mater. **27**, 7314–7319 (2015).

Reuse of AIP Publishing content is subject to the terms: https://publishing.aip.org/authors/rights-and-permissions. Downloaded to IP: 91.252.167.84 On: Thu, 04 Aug 2016 20:13:45